Concepts

Emphasizing new ideas to stimulate research in ecology

Editor's Note

Invasions of new territory—by plants, animals, or genes—are an old topic in ecology, but hardly obsolete: the spread of pests such as the gypsy moth, exotic plants, recurrent and emerging infectious diseases, and genetically engineered organisms are important contemporary problems for ecology. For nearly half a century, reaction–diffusion models have been the main analytic framework for modeling spatial spread, in part because of the well-developed mathematical theory that tells us how to compute things like the long-term rate of spread and the conditions for spatial pattern formation. In this paper, we are given the tools to study the rate of spread for invading organisms in a very different kind of model, integrodifference equations. Unlike diffusion equations, these models can accommodate leptokurtic (broad-tailed) dispersal patterns, and in such cases they can exhibit the accelerating rates of spread that have been observed in some invasions. Of course this does not mean that we should stop using diffusion models, but it gives us an alternative with a different set of assumptions that is likely to be more accurate when the dispersal pattern of individuals is far from the Gaussian distribution implicit in a diffusion model.

Stephen P. Ellner

Ecology, 77(7), 1996, pp. 2027–2042

DISPERSAL DATA AND THE SPREAD OF INVADING ORGANISMS[1]

Mark Kot
Department of Mathematics, University of Tennessee, Knoxville, Tennessee 37996-1300 USA

Mark A. Lewis
Department of Mathematics, University of Utah, Salt Lake City, Utah 84112 USA

P. van den Driessche
Department of Mathematics and Statistics, University of Victoria, Victoria, British Columbia, V8W 3P4 Canada

Abstract

Models that describe the spread of invading organisms often assume that the dispersal distances of propagules are normally distributed. In contrast, measured dispersal curves are typically leptokurtic, not normal. In this paper, we consider a class of models, integrodifference equations, that directly incorporate detailed dispersal data as well as population growth dynamics. We provide explicit formulas for the speed of invasion for compensatory growth and for different choices of the propagule redistribution kernel and apply these formulas to the spread of *D. pseudoobscura*. We observe that: (1) the speed of invasion of a spreading population is extremely sensitive to the precise shape of the redistribution kernel and, in particular, to the tail of the distribution; (2) fat-tailed kernels can generate accelerating invasions rather than constant-speed travelling waves; (3) normal redistribution kernels (and by inference, many reaction-diffusion models) may grossly underestimate rates of spread of invading populations in comparison with models that incorporate more realistic leptokurtic distributions; and (4) the relative superiority of different redistribution kernels depends, in general, on the precise magnitude of the net reproductive rate. The addition of an Allee effect to an integrodifference equation may decrease the overall rate of spread. An Allee effect may also introduce a critical range; the population must surpass this spatial thresh-

[1] Manuscript received 8 March 1995; revised 2 November 1995; accepted 21 December 1995.

old in order to invade successfully. Fat-tailed kernels and Allee effects provide alternative explanations for the accelerating rates of spread observed for many invasions.

Key words: Allee effect; biological invasions; dispersal; integrodifference equations; seed shadows; spatial models.

Introduction

Dispersal patterns have been measured for a tremendous number of organisms, either as seed shadows (Okubo and Levin 1989, Carey and Watkinson 1993, Willson 1993), plant-disease dispersal gradients (Kiyosawa and Shiyomi 1972, Kable et al. 1980, Lambert et al. 1980; McCartney and Bainbridge 1984, Grove et al. 1985, Mundt and Leonard 1985, Fitt et al. 1987, Mundt 1989), or mark–recapture data (Dobzhansky and Wright 1943, Wolfenbarger 1946, 1959, 1975, Taylor 1978, Makino et al. 1987). There is tremendous variability in these data. At the same time, there is one overwhelming regularity: the spatial distribution of propagules about a source is typically leptokurtic (Bateman 1950, Wallace 1966, Okubo 1980, Howe and Westley 1986, Willson 1992), with more propagules near the center and in the tails than in a normal distribution of comparable mean and variance. Indeed, dispersal data are frequently fit with a negative exponential curve or with a negative power function (McCartney and Bainbridge 1984, Fitt et al. 1987, Okubo and Levin 1989, Willson, 1993).

All too often, this pattern is ignored. Analyses of the spread of invading organisms (Okubo 1980, Roughgarden 1986, Williamson 1989, Hengeveld 1994) frequently start with a simple reaction–diffusion model with exponential growth and Fickian diffusion. This model, introduced by Skellam (1951) to describe the spread of muskrats, is at odds with much of the dispersal data: individuals are assumed to disperse in each direction with equal probability and with the dispersal distance *normally* (rather than leptokurtically) distributed.

How *should* one proceed? Mollison (1977) has argued for continuous-time models built around probability (or contact) distributions for the distance that an individual moves. Spatial contact models incorporate a variety of contact distributions, including the leptokurtic distributions that are so prevalent in the dispersal data. Continuous-time spatial contact models have been studied extensively with regard to epidemics (Kendall 1965, Mollison 1972*a, b,* Atkinson and Reuter 1976, Brown and Carr 1977). The recent addition of age structure to these models (van den Bosch et al. 1990, Mollison 1991) has, in turn, prompted keen ecological interest (Hengeveld 1994).

There are also discrete-time contact models. These models have a remarkably long history. They are at the heart of the problem of random flights (Pearson 1905, Markoff 1912, Chandrasekhar 1943) wherein a particle undergoes a sequence of independent and random displacements of given distribution. Slatkin (1973), Weinberger (1978, 1982), and Lui (1982*a, b,* 1983) used such models to predict changes in gene frequency. More recently, they have appeared in population ecology, as integrodifference equations (Kot and Schaffer 1986, Hardin et al. 1990, Kot 1989, 1992, Andersen 1991, Hastings and Higgins 1994, Neubert et al. 1995) for populations with discrete nonoverlapping generations and well-defined growth and dispersal stages.

Some of the best dispersal data occur for monocarpic plants and semelparous insects. Many of these organisms have discrete nonoverlapping generations and well-defined growth and dispersal stages. We focus, therefore, on discrete-time spatial contact models—alias integrodifference equations. We are interested in the rate of spread of invading organisms. We are particularly interested in the sensitivity of the speed of invasion to changes in the contact distribution (redistribution kernel) and to changes in the growth dynamics.

In the section *Model,* we outline a simple discrete-time model for the growth and spread of organisms. We begin with simple density-dependent growth; we incorporate dispersal data directly into the model by means of a redistribution kernel. The shape of this redistribution kernel has a profound impact on the speed of invasion. We summarize various formulas for this speed in the *Analytic results* section. The detailed derivation of these formulas is relegated to Appendix A. In the section *Empirical example,* we reexamine the insect dispersal data of Dobzhansky and Wright (1943) and compare the rates of spread for five distinct redistribution kernels that fit this data. Critical depensation in growth may also have a profound effect on the speed and success of invasions. We analyze a tractable model that incorporates such an Allee effect in the section *Spread with Allee effect* and in Appendix B. We discuss the implications of our results in the *Discussion.*

Model

We begin with a population in which individuals grow and disperse, in synchrony, on a continuous one-dimensional habitat. There is a sedentary stage and a dispersal stage. All growth occurs during the sedentary stage; all movement occurs during the dispersal stage.

For the sedentary stage, we begin with a simple nonlinear difference equation

$$N_{t+1} = f(N_t) \tag{1}$$

such as the Beverton–Holt stock–recruitment curve (Beverton and Holt 1957, Pielou 1977, Prout 1978)

$$N_{t+1} = \frac{R_0 N_t}{1 + [(R_0 - 1)/K]N_t}, \tag{2}$$

or the Ricker (1954) curve

$$N_{t+1} = N_t \exp\left[r\left(1 - \frac{N_t}{K}\right)\right]. \tag{3}$$

In the above equations, N_t is the population level at time t, K is the carrying capacity of the environment, R_0 is the net reproductive rate, and r is the intrinsic rate of increase. The exact form of $f(N_t)$ will not matter as long as it is nonnegative and satisfies

$$f(N) \leq f'(0)N. \tag{4}$$

In particular, we assume that there is no Allee effect. We will relax this restriction in the section *Spread with Allee effect.*

Eq. 1 does not account for the dispersion of the population. To amend this situation, we let $N_t(x)$ represent the population density as a function of space at the start of the t^{th} generation. We imagine that change occurs in two distinct stages. (1) During the sedentary stage, $N_t(x)$ is mapped into $f[x, N_t(x)]$. Explicit spatial dependence, henceforth dropped, reflects clinal (spatially varying, time-independent) variation in the parameters. (2) Progeny then disseminate. We describe the details of this movement with a linear integral operator that tallies movement from all y to all x. Together, these two stages yield the integrodifference equation

$$N_{t+1}(x) = \int_{-\infty}^{+\infty} k(x, y) f[N_t(y)]\, dy \tag{5}$$

for the growth and dispersal of the population on an infinite one-dimensional domain.

The redistribution kernel $k(x, y)$ describes the dispersal of the population. In particular, $k(x, y)$ is the probability density function for propagules dispersing from a source at position y. The kernel $k(x, y)$ must remain nonnegative. It may, however, depend on absolute location or only on relative distance. In the latter case, Eq. 5 features a convolution integral:

$$N_{t+1}(x) = \int_{-\infty}^{+\infty} k(x - y) f[N_t(y)]\, dy. \tag{6}$$

We will restrict our attention to convolution integrals throughout the remainder of this paper.

The two assumptions, that the growth function f depends only on N_t and that the redistribution kernel depends only on $x - y$, imply that the habitat is homogeneous and that the growth and dispersal properties are the same at each point in space. Methods for measuring the relevant ecological data and for estimating the kernel from observed data are discussed in Southwood (1978), Silverman (1986), and Tarter and Lock (1993). We will say more about the shape of redistribution kernels in the sections *Analytic results* and *Empirical example.*

Analytic Results

We have claimed that the exact form of $f(N_t)$ in Eq. 6 does not matter. There is compelling evidence that the asymptotic velocity of expansion of a nonlinear (differential or integral) model is the same as that of its linearization. The continuous-time version of this broad principle has been referred to as the *linear conjecture* (Mollison 1991). It is expected to hold if (a) an individual's reproduction in an "occupied" environment is always less than in a "virgin" environment (i.e., no critical depensation or Allee effect), and (b) the influence of an individual on the environment far from its (present) position is negligible (i.e., no long-distance density dependence) (van den Bosch et al. 1990, Mollison 1991).

For integrodifference equations, this same principle would imply that we may infer the velocity of Eq. 6 from the linear integrodifference equation

$$N_{t+1}(x) = f'(0) \int_{-\infty}^{+\infty} k(x - y) N_t(y)\, dy. \tag{7}$$

Weinberger (1978, 1982) has proven this result for models with monotonically increasing growth functions. In addition, Eq. 4 guarantees us that the rate of spread will be at most that of Eq. 7, even with overcompensation (Clark 1990) or scramble competition (Hassell 1975).

Despite this tremendous simplification, integrodifference equations may still exhibit a wide variety of solutions and a wide range of velocities for different choices of the redistribution kernel $k(x - y)$. There are three important classes of redistribution kernels:

1. *The kernel* k(x) *has a moment-generating function.*—That is, the moment-generating function

$$M(s) = \int_{-\infty}^{+\infty} k(x) e^{sx}\, dx \tag{8}$$

exists for some interval of s about zero.

These are kernels with exponentially bounded tails. Nonlinear integrodifference equations built with these

kernels typically possess travelling wave solutions (Weinberger 1978, 1982, Lui 1982*a*, *b*, 1983, Kot 1992). For a given kernel, the minimum speed c of a rightward moving wave of invasion will depend upon the net reproductive rate R_0 [we have taken $f'(0) = R_0$; see Eq. 2]. The curve relating these two quantities may be written parametrically as

$$c = \frac{M'(s)}{M(s)}, \tag{9a}$$

$$R_0 = \frac{e^{sM'(s)/M(s)}}{M(s)} \tag{9b}$$

(see Appendix A).

For example, the normal distribution

$$k(x) = \frac{1}{\sigma\sqrt{2\pi}} e^{-x^2/2\sigma^2} \tag{10}$$

has a moment-generating function of the form

$$M(s) = e^{\sigma^2 s^2/2}. \tag{11}$$

In this case, Eqs. 9a, b reduce to

$$c = \sigma^2 s, \tag{12a}$$

$$R_0 = e^{\sigma^2 s^2/2}, \tag{12b}$$

or, equivalently, to

$$c = \sigma\sqrt{2 \ln R_0}. \tag{13}$$

If one identifies

$$r \equiv \ln R_0, \tag{14a}$$

$$D \equiv \frac{\sigma^2}{2}, \tag{14b}$$

one recaptures the speed of invasion,

$$c = 2\sqrt{Dr}, \tag{15}$$

first derived by Fisher (1937) for the reaction-diffusion equation

$$\frac{\partial N}{\partial t} = rN\left(1 - \frac{N}{K}\right) + D\frac{\partial^2 N}{\partial x^2}. \tag{16}$$

Other kernels (e.g., Neubert et al. 1995) yield other speeds of invasion.

2. *The kernel* k(x) *has finite moments,*

$$\mu_n' = \int_{-\infty}^{+\infty} x^n k(x)\, dx, \tag{17}$$

of all orders n, *but no moment-generating function.*— These are fat-tailed kernels. Mollison (1972*b*) has shown (for continuous-time models) that kernels lacking exponentially bounded tails generate asymptotically infinite velocities of expansion. We can be quite precise about the manner in which infinite velocities are reached for integrodifference equations. If the redistribution kernel satisfies a certain technical condition, (Eq. A.27), the fundamental solution of Eq. 7, corresponding to an initial point source of strength N_0, satisfies

$$N_t(x) \sim N_0 R_0' k(x), \quad |x| \gg 1, \quad t \geq 1 \tag{18}$$

for large x (see Appendix A). If we now define the *extent* of the population as the distance from the source where the population first falls below a given threshold, $N_t = \bar{N}$, $\bar{N}$ sufficiently small, it follows that the extent at time t, x_t, is given by inverting Eq. 18 for $N_t = \bar{N}$. That is, the extent is either

$$x_t = k^{-1}\left(\frac{\bar{N}}{N_0 R_0'}\right), \tag{19}$$

with k^{-1} the inverse of k, or zero (if the population is always below $\bar{N}$).

For example, a population with redistribution kernel

$$k(x) = \frac{\alpha^2}{4} e^{-\alpha\sqrt{|x|}} \tag{20}$$

(see section *Empirical example*) has a spatial extent

$$x_t = \frac{1}{\alpha^2}\left[(\ln R_0)t + \ln\left(\frac{\alpha^2 N_0}{4\bar{N}}\right)\right]^2 \tag{21}$$

that grows quadratically with time. The velocity of expansion grows linearly with time.

3. *The kernel* k(x) *has moments that are infinite.*— These are extremely fat-tailed kernels. So much so, that Approximation 18 fails. However, one can still make considerable progress in analyzing Eq. 7 using Fourier transforms and characteristic functions (see Appendix A). For one well-known kernel, Eq. 7 may even be solved exactly. The Cauchy distribution,

$$k(x) = \frac{1}{\pi}\frac{\beta}{(\beta^2 + x^2)} \tag{22}$$

(with no moments of positive integral order) has a fundamental solution, corresponding to a point source of strength N_0, of the form

$$N_t(x) = \frac{\beta t}{\pi(\beta^2 t^2 + x^2)} N_0 R_0'. \tag{23}$$

In this instance, the spatial extent of the population,

$$x_t = \sqrt{\frac{\beta t N_0 R_0'}{\pi \bar{N}} - \beta^2 t^2}, \tag{24}$$

grows faster than geometrically. For $f(N_t) = N_t$, organisms follow a Levy walk (Weiss 1994).

Empirical Example

One of the earliest quantitative studies of insect dispersal was Dobzhansky and Wright's (1943) study of genetically marked *Drosophila pseudoobscura*. Dobzhansky and Wright analyzed their data in terms of the normal distribution, although they realized that the actual distribution was leptokurtic. Bateman (1950) questioned whether dispersing *Drosophila* are, in fact, normally distributed; he also tested for leptokurtosis. Wallace (1966) reanalyzed the Dobzhansky and Wright data and showed that they fit a leptokurtic model in which the log of the number of recaptured flies decreased linearly with the square root of distance from the point of release. Taylor (1978) compared the effectiveness of eight different models in fitting the data and reaffirmed Wallace's result.

Three of Taylor's curves (5, 6, and 8) integrate to infinity (even though there were only a finite number of flies released) and cannot be used for redistribution kernels. However, the other five curves (1, 2, 3, 4, and 7) do have finite integrals. These five dispersal curves are shown in Fig. 1. The first curve is a parametric form of the normal distribution. Curves 2 and 3 were used by Wolfenbarger (1946, 1959, 1975) in his extensive analyses of dispersal data. Curve 4 is Wallace's (1966) model for the dispersal of *D. pseudoobscura*. Finally, curve 7 is a parametric form of the Laplace distribution. Curve 4 provides the best fit to the data; curve 1 fits the data rather poorly.

Taylor's models provide us with five plausible descriptions of lifetime dispersal in *Drosophila pseudoobscura*. We have normalized these curves and formed five redistribution kernels. These kernels appear as probability density functions 1, 2, 3, 4, and 7 in Fig. 1.

To construct a model for invading drosophilids, we must also account for growth. Prout (1978) has advocated the use of the Beverton–Holt curve (Eq. 2) as a growth model for insects. This curve is consistent with the dynamic stability of drosophilid populations observed by Thomas et al. (1980), Pomerantz et al. (1980), and others. We use the Beverton–Holt curve throughout this section. However, two-stage models that describe density dependence among both preadults and adults (Prout and McChesney 1985, Rodriguez 1988) could also be used.

The actual spread was in two dimensions, but we treated the problem as one dimensional for convenience, and because one-dimensional models typically recapitulate the long-term features of axisymmetric spread (Murray 1989). In particular, we took the Beverton-Holt curve (Eq. 2) and combined it with each of the five probability density functions in Fig. 1 to form five integrodifference equations (not shown, but see Eq. 6). Fig. 2 shows the solutions that result from iterating each of these five integrodifference equations numerically for the same point-source initial condition. The solutions are superficially rather similar. Models 1, 2, 3, and 7 (the four integrodifference equations containing density functions 1, 2, 3, and 7) rapidly generate travelling waves that preserve their shape and that move across space with constant velocity. However, the solutions for model 4 continue to change, both in shape and speed. There are also significant differences in spatial scale for all five models. These differences are accentuated in Fig. 3. This figure shows the extent of each population as a function of time (in generations). For models 1, 2, 3, and 7, the spatial extent increases linearly with time. The slope of each straight line is the speed of invasion (c) for that kernel. The spatial extent for model 4 increases quadratically with time.

Probability density functions 1, 2, 3, and 7 have exponentially bounded tails. They belong to our first class of redistribution kernels. We expect each of these kernels to yield models with constant-speed travelling waves; our numerical simulations indicate that they do. Eqs. 9a, b allow us to compute the speed of invasion as a function of the net reproductive rate R_0 for each of these four density functions. These curves are displayed in Fig. 4. The speeds of invasion for density functions 2 and 3 exceed that of density function 7 for low values of R_0. However, the speed for density function 7 surpasses that for density functions 2 and 3 at higher net reproductive rates. The best-fitting normal distribution provides the lowest estimate of the speed of invasion for all of the plotted reproductive rates.

Probability density function 4 is in our second class of redistribution kernels. Indeed, it is just Eq. 20 with $\alpha = 6.730678$. There is no longer a constant speed of invasion for each value of R_0. Rather, this speed increases with time. Even so, Eq. 21 provides an accurate description of the spatial extent for each time and for each value of R_0. For example, Eq. 21 (with $\alpha = 6.730678$, $R_0 = 10.0$, $N_0 = 50/32767$, and $\bar{N} = 0.05$) provides an excellent fit (see Fig. 5) to the numerically computed curve in Fig. 3.

Spread with Allee Effect

When the reproductive dynamics exhibit an Allee effect (critical depensation) the linear conjecture of the *Analytic results* section no longer holds. In this case the wave is no longer "pulled" by the leading edge of the wave, but is "pushed" by individuals reproducing at higher densities and spilling outwards (via the redistribution kernel) at densities sufficient to

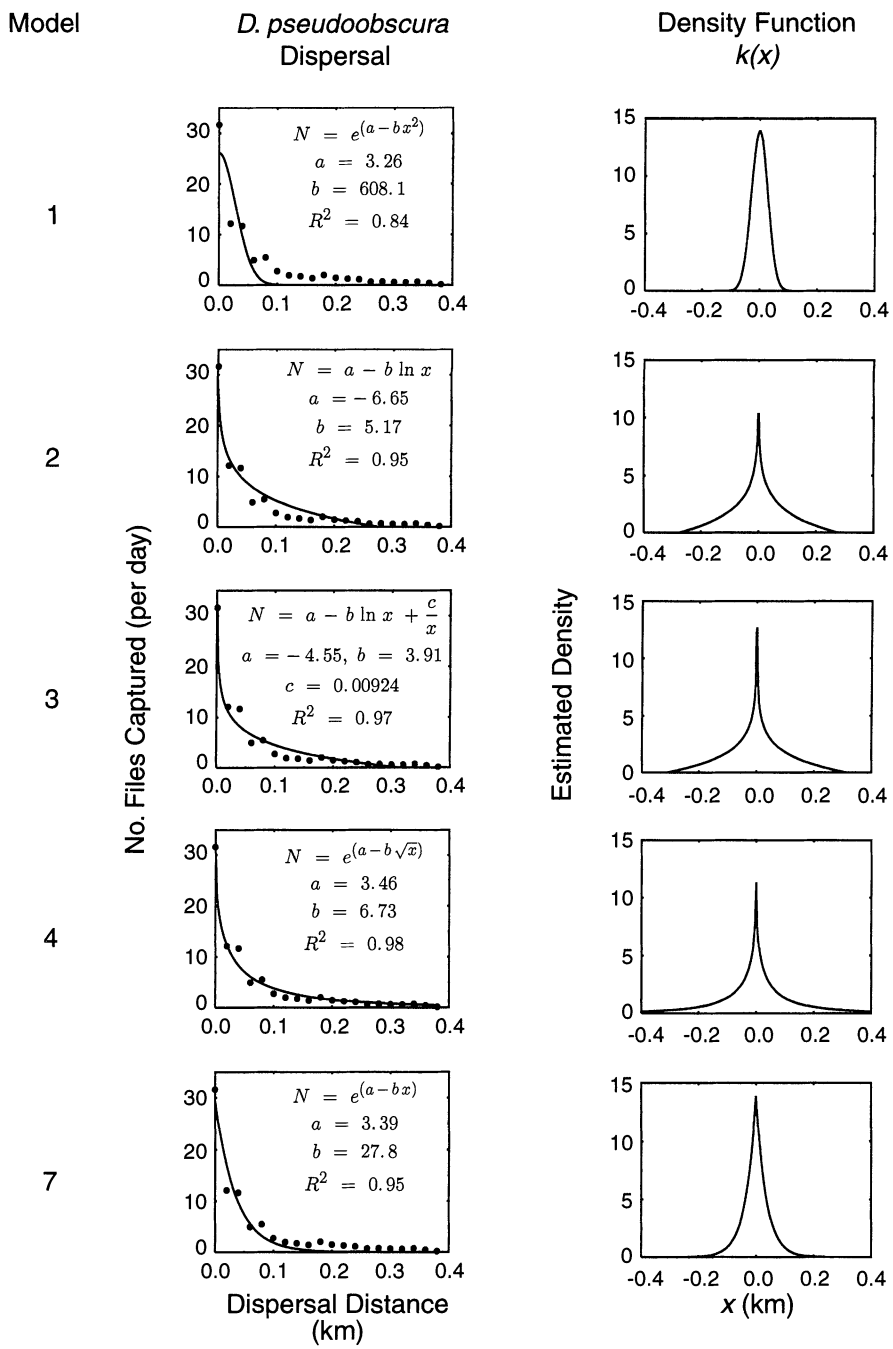

FIG. 1. Dispersal curves and redistribution kernels for *D. pseudoobscura*. The left half of the figure shows data for the number of *D. pseudoobscura* captured per trap-day and a set of fitted curves. The curves are taken from Taylor (1978). The parameters differ from those of Taylor (1978) because of our use of kilometres rather than metres. The curves have similar coefficients of determination (R^2) but differ significantly in their tails. For each dispersal curve we have also drawn, on the right, the corresponding redistribution kernel. To obtain this curve, we mirrored each dispersal curve about the origin and divided by the total area underneath the curve so as to generate a probability density function with total area equal to 1.

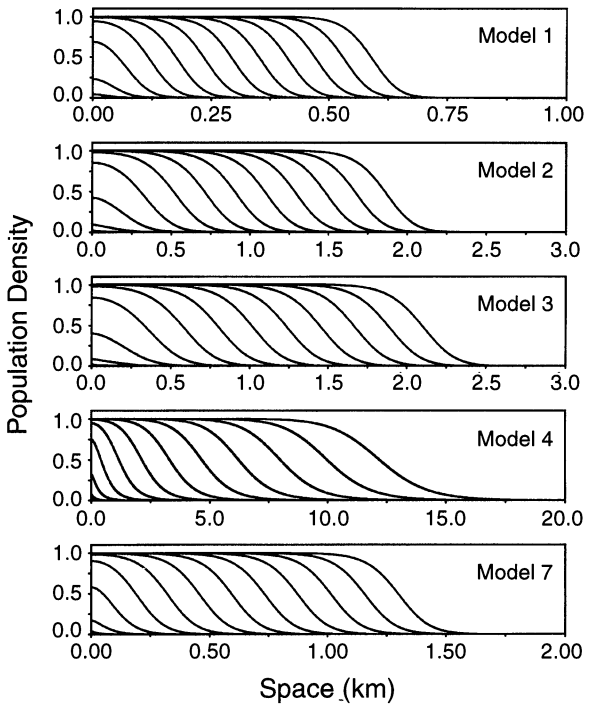

FIG. 2. Simulated solutions to Eq. 6 for each of the five redistribution kernels in Fig. 1 and for growth governed by the Beverton–Holt curve with $R_0 = 10.0$. Each integrodifference equation was iterated for 12 generations starting with an initial point source of strength $N_0 = 50/32\,767$ centered at the origin. The integrodifference equations were integrated using a fast-Fourier-transform-assisted implementation of the extended trapezoidal rule on a domain of length 50 with 32 768 grid points. Integrodifference equations built with density functions 1, 2, 3, and 7 rapidly generate travelling waves that preserve their shape and that move across space with constant velocity. In contrast, the "wave of invasion" in simulation 4 continues to accelerate.

overcome the threshold for population growth (N_c) (Fig. 6).

There is no easy general method for calculating this spread rate (but see Weinberger 1982, Lui 1983). Hence, to highlight the influence of an Allee effect we use a piecewise constant approximation to the growth function (see horizontal dashed lines in Fig. 6). We couple this to a general redistribution kernel. For this particular model, it is easy to calculate the spread rate, as shown below and in Appendix B.

We assume that a very large (semi-infinite) area has been colonized and that $N_0(x)$ lies below the Allee threshold (N_c) to the left of some point x_t and above N_c to the right of x_t. Integrodifference Eq. 6 then simplifies to

$$N_{t+1}(x) = K \int_{x_t}^{\infty} k(x - y)\, dy = KF(x - x_t), \quad (25)$$

where $F(x)$ is the cumulative distribution function (CDF),

$$F(x) = \int_{-\infty}^{x} k(y)\, dy, \quad (26)$$

and K is the carrying capacity for the population (see Fig. 6). Another iteration yields a further translation of the function on the right-hand side of Eq. 25. Thus the shape of the wave front is given by the cumulative distribution function for the kernel. The distance invaded in one generation, $x_t - x_{t+1}$, is given by Eq. 25 as

$$F(x_{t+1} - x_t) = \frac{N_c}{K}. \quad (27)$$

Fig. 7 shows us that, with the above formula, the population is spreading ($x_t - x_{t+1} > 0$) if $N_c < KF(0)$ and is retreating ($x_t - x_{t+1} < 0$) if $N_c > KF(0)$. In the case of a symmetric kernel [$F(0) = 1/2$], the range expands if the Allee threshold N_c is below half the carrying capacity and retreats if the Allee threshold is above half the carrying capacity.

We can apply our results to the kernels for *D. pseudoobscura* plotted in Fig. 1. As motivation for doing so, we note that although drosophilids typically exhibit compensatory growth, the introduction of sterile males may introduce an Allee effect (Prout 1978, Lewis and van den Driessche 1993). Given the simplified Allee growth dynamics analyzed here, we can easily calculate the distance invaded per generation for any

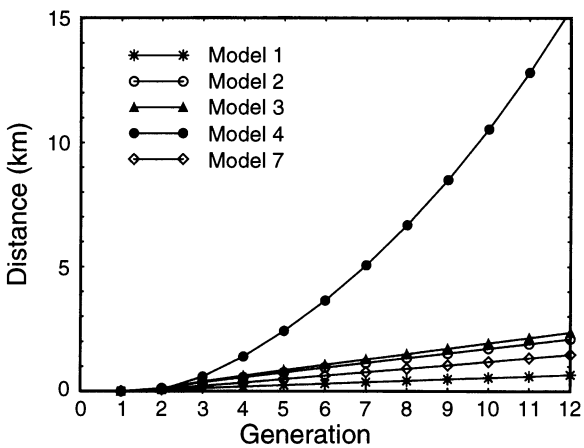

FIG. 3. The extent of each population in Fig. 2 is plotted as a function of time. The spatial extent was computed by finding the distance from the source where the population first reached the threshold $\bar{N} = 0.05$. For models 1, 2, 3, and 7, the spatial extent increases linearly with time. However, for model 4, this measure increases as a quadratic function of time.

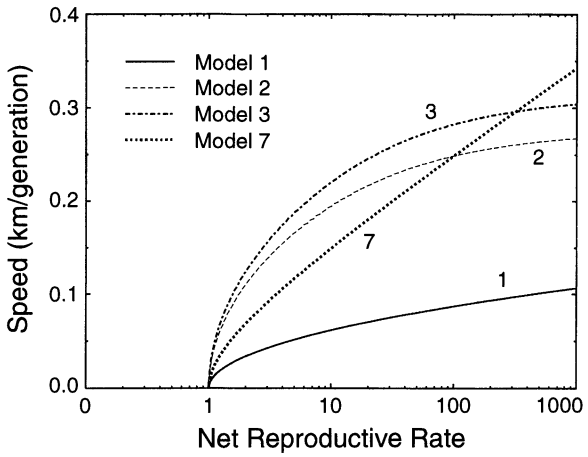

FIG. 4. The speed of invasion as a function of the net reproductive rate R_0 for the four probability density functions 1, 2, 3, and 7 (see Fig. 1). Each curve was computed using parametric Eqs. 9a, b. The best-fitting normal distribution (density function 1) provides the lowest estimate of the speed of invasion for all plotted reproductive rates. Density function 4 was not included in this figure since it generates accelerating wavefronts rather than constant-speed travelling waves.

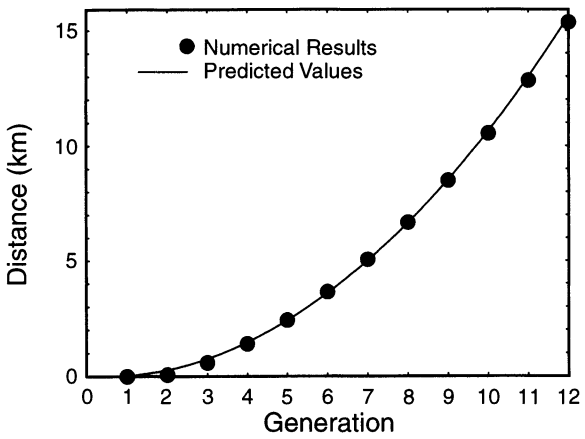

FIG. 5. A comparison between an analytic approximation for the spatial extent of an accelerating invader and the actual extent that was observed in numerical simulations. The numerical values were obtained by simulating Eq. 6 with the redistribution kernel (Eq. 20) under conditions described in Fig. 2 and with $R_0 = 10.0$, $\alpha = 6.730678$, and $\bar{N} = 0.05$. The analytic approximation was Eq. 21 with R_0, α, and $\bar{N}$ as above. The analytic approximation does an excellent job of predicting the numerically calculated course of invasion.

threshold N_c (as shown in Fig. 8). It is interesting to note that while the rank orderings for invasion rates are effectively the same as those given in Fig. 4, the fat-tailed kernel (Eq. 4) now has a finite invasion speed. However, for small thresholds, this speed is quite large.

We now consider a population that initially occupies a small interval. We define the population range at time t, $2x_t$, as that length of interval within which the population level exceeds the growth threshold N_c; we choose the space coordinate so that it is centered on the middle of this range. In Appendix B (see also Fig. 9) we show that the initial range, $2x_0$, determines whether the range increases or decreases with time. The critical spatial extent x_c, which neither increases nor decreases with time, is given by

$$F(2x_c) = F(0) + \frac{N_c}{K} \qquad (28)$$

(Fig. 7). A simple method of predicting the success of an invasion in terms of the cumulative distribution function (Eq. 26), the Allee threshold (N_c), the carrying capacity (K), and the initial range ($2x_0$) is thus to compare $F(2x_0)$ with $F(0) + N_c/K$. If $F(2x_0)$ is larger, then x_0 is larger than x_c (Fig. 7) and the invasion will succeed. Otherwise, the invasion will fail, collapsing inwards upon itself.

In Appendix B we also derive a recurrence relationship between x_{t+1} and x_t for the Laplace redistribution kernel. The rate of spread from generation to generation is shown in Fig. 10.

In summary, we note that the invasion will always fail if the Allee threshold is too high [$N_c > KF(0)$]. However, even with a low Allee threshold, there is a

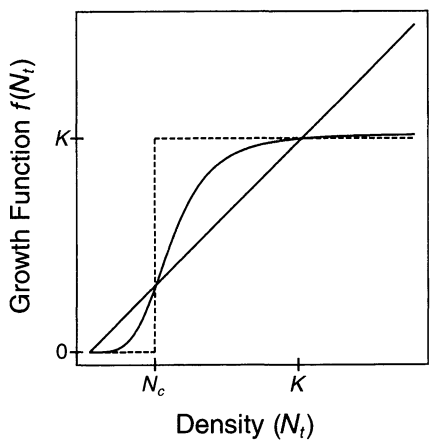

FIG. 6. The Allee growth function $f(N_t)$ as a function of the population density N_t. The function satisfies $N_{t+1} = f(N_t)$, and the diagonal line satisfies $N_{t+1} = N_t$. Note that $f(N_t)$ is below the diagonal for $0 < N_t < N_c$ and that it is above the diagonal for $N_c < N < K$. The solution to the difference equation $N_{t+1} = f(N_t)$ can be obtained graphically by "cobwebbing." Note also that populations below N_c go extinct, while populations initially above N_c approach the carrying capacity K. The dashed line shows a piecewise constant approximation to f.

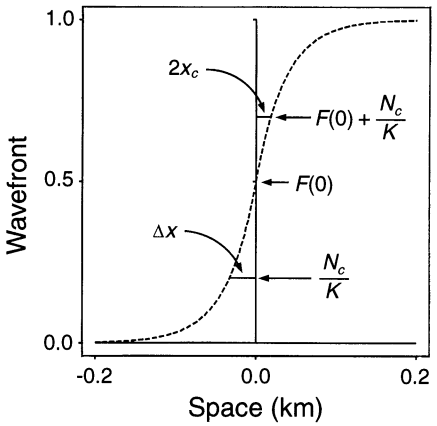

FIG. 7. The cumulative distribution function of the redistribution kernel (Eq. 26) can be used to calculate asymptotic rate of spread per generation ($\Delta x = x_{t+1} - x_t$) and the critical range $2x_c$ that a population must surpass in order to invade. Refer to Eqs. 27 and 28. The cumulative distribution function in this figure corresponds to the Laplace redistribution kernel in Fig. 1 (density function 7) with $b = 27.8$; the threshold N_c/K has been set to 0.2. As a result, $\Delta = -0.0330$ km, $F(0) = 0.5$, and $2x_c = 0.0184$ km.

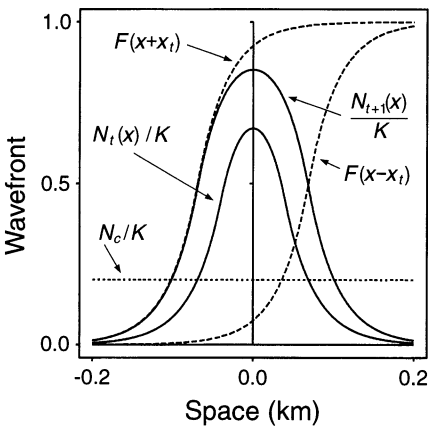

FIG. 9. The population density at time $t + 1$, $N_{t+1}(x)$, can be derived graphically from the corresponding population density $N_t(x)$ at time t. $N_t(x) = N_c$ determines the population's spatial extent x_t. This is used to evaluate two horizontally translated cumulative distribution functions, $F(x + x_t)$ and $F(x - x_t)$, of the redistribution kernel. Finally, Eq. B.2 gives the $N_{t+1}(x)/K$ as the difference between the two distribution functions. The redistribution kernel and Allee threshold N_c/K are identical to those in Fig. 6. The spatial extent x_t was chosen to be 0.0688 km, and thus $x_{t+1} = 0.101$ km.

spatial threshold for the range ($2x_c$) given by Eq. 28; the population must surpass this threshold if the invasion is to succeed. Also, just past this threshold, the invasion starts slowly; it then accelerates before asymptotically approaching a constant velocity. For a successful invasion, the spreading wave front is (asymptotically) the cumulative distribution function for the dispersal kernel.

Aronson and Weinberger (1975) have shown that similar thresholds exist for certain classes of reaction-diffusion models in one spatial dimension; these thresholds have been analyzed geometrically (in two spatial dimensions) by Lewis and Kareiva (1993).

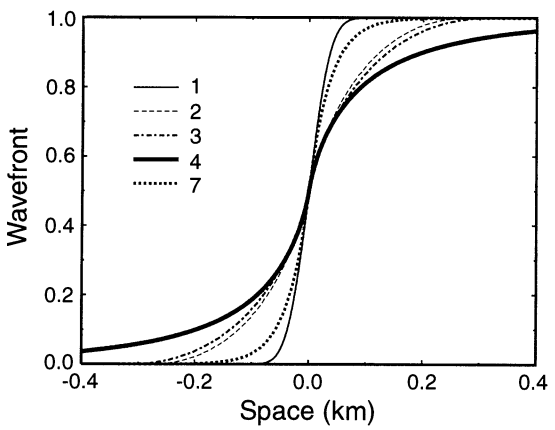

FIG. 8. Cumulative distribution functions for the five *D. pseudoobscura* redistribution kernels of Fig. 1. For an idealized Allee effect, the rate of spread is determined by the abscissa of the point of intersection of the cumulative distribution function with the horizontal line of height N_c/K (see Fig. 7). Increasing the threshold N_c decreases the rate of spread.

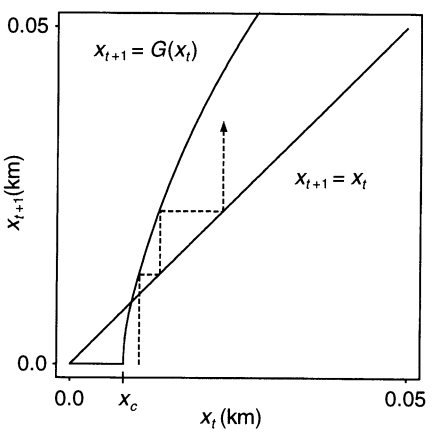

FIG. 10. A mapping for spatial extent as a function of time. $G(x_t)$ is the mapping that prescribes the spatial extent at time $t + 1$ in terms of the spatial extent at time t. If $x_0 < x_c$, the range falls to 0, whereas if $x_0 > x_c$, the rate of spread increases and asymptotically approaches a constant velocity. Refer to Eqs. B.8 and B.10. The redistribution kernel, N_c/K, and x_c are as given in Fig. 6.

Discussion

There are several conclusions that follow from the general analyses of the *Analytic results* and *Spread with Allee effect* sections and from the detailed example of the *Empirical example* section:

1) The speed of invasion of a spreading population is quite sensitive to the shape of the redistribution kernel. Kernels with similar coefficients of determination will yield dramatically different speeds if they differ significantly in their tails.

This would appear to be an especially vexing problem for various model-free curve estimation procedures. A probability density may, for example, be estimated from a sample by replacing each data-point by a kernel function (not to be confused with the redistribution kernel) of fixed window width or bandwidth. This kernel-based estimation procedure is a simple generalization of the usual histogram. However, because the window width is fixed across the entire sample, there is a tendency for spurious noise to appear in the tails of the estimates of long-tailed distributions (Silverman 1986). If the estimates are smoothed to deal with this, essential details in the main part of the distribution are often masked. Also, there appears to be little difference between commonly chosen kernels with regard to minimizing mean integrated square error (Tarter and Lock 1993). Density estimation researchers may, as a result, feel that the shape of the kernel function is not of crucial importance. However, different kernel functions will typically generate probability density functions with very different tails.

2) Solutions to integrodifference equations may display accelerating rates of spread. Fat-tailed kernels that lack exponentially bounded tails give rise to accelerating invasions. Populations escaping an Allee effect may temporarily accelerate prior to attaining a constant speed.

How seriously should one take fat-tailed kernels and the resulting prediction of accelerating invasions? One reasonable approach is to argue that any infinite tail, whether Gaussian or fat, is clearly unrealistic. Any reasonable biological model for spread will have an upper bound for the distance that one propagule can travel. As a result, all reasonable redistribution kernels should vanish outside some bounded set, and thus have no tail at all. Truncating a tail, in turn, leads us back to a constant (though possibly high) speed of invasion.

More to the point, there is danger in extrapolating any set of dispersal data. The *D. pseudoobscura* data in Fig. 1 is for distances of up to 0.38 km. Extrapolating to distances far beyond this is perilous.

At the same time, certain groups of organisms do appear to have long-tailed redistribution kernels. It is common in plant pathology and plant disease epidemiology to fit negative power laws to the dispersal of air-borne fungal, bacterial, and viral spores. Of 124 dispersal gradients measured for dry airborne spores or pollen and included in the review by Gregory (1968), 59 were fit better by a negative power law and 65 were fit better by a simple exponential model (Fitt and McCartney 1986). In a later and more exhaustive analysis of 325 data sets, Fitt et al. (1987) conclude that there is generally little difference between these two models in the goodness of fit to these data, although gradients for fungi with air-borne spores less than 10 μm in diameter were fit better by power law models.

Fitt et al. (1987) warn against extrapolating spore dispersal data outside their observed range, and yet the phytopathology literature is replete with discussions and examples of the importance of long-distance dispersal (Aylor 1986, Pedgley 1986, Nagarajan and Singh 1990). Minute spores may remain airborne, carried by the wind, for days. One of the most fascinating examples concerns the spread of spores of *Puccinia graminis* var. *tritici* (the causal agent of wheat stem rust) (Roelfs 1985, Aylor 1986, Pedgley 1986). The uredial stage of this rust does not survive the winter north of Texas and is unable to survive the summer in Texas. It persists by spreading northward in spring and early summer and southward in late summer and fall. In 1923, it spread northward at ≈54 km/d. In 1925, on the other hand, rust appeared almost simultaneously over a distance of 970 km, suggesting that one massive spore shower may have brought inoculum to the entire region. The longest well-documented single movement of urediospores in North America was at least 680 km, between two wheat-growing regions in Canada separated by forest, lakes, and tundra (Roelfs 1985). Other examples include the spread of *Puccinia polysora* (the causal agent of maize rust) across Africa from 1949 to 1953 (Rainey 1973), the possible introduction of *Hemileia vastastrix* (the causal agent of coffee leaf rust) from Angola into Brazil by one weather event (Bowden et al. 1971), the sudden and rapid spread of coffee rust across South America (Schieber 1972, 1975, Waller 1979), the apparent transport of urediospores of *Puccinia melanocephala* (the causal agent of sugarcane rust) from the Cameroons in West Africa to the Dominican Republic in the Caribbean over the course of 9 d (Purdy et al. 1985), and the subsequent rapid spread of this rust throughout the Americas in the next year.

Minogue (1989) has also argued, on theoretical grounds, for the use of the fat-tailed Pareto distribution for data that show no convergence toward constant estimates of the mean and variance (of dispersal dis-

tance) over practical scales of observation. He has also emphasized that even when the majority of spores land close to the source and only a tiny proportion travel long distances, as is common among wind-dispersed pathogens, it is that tiny proportion that determines the rate of spatial spread. Shaw (1994), in turn, has argued that the fat-tailed Cauchy distribution (see Eq. 22) is just the kind of redistribution kernel that phytopathologists should be studying to understand certain unpredictable plant pathogens.

In the real world, all spreading populations must eventually slow down. They may, nonetheless, exhibit an initial period in which the range expansion rate is increasing and curvilinear. This is the case, for example, with the historical spread of the Japanese beetle (*Popillia japonica*) and of the European Starling (*Sturnus vulgaris*) in eastern North America (Elton 1958, Hengeveld 1989) as well as for many of the plant pathogens that we have mentioned. (See Shigesada et al. [1995] for additional examples and for a recent discussion of this topic.) One possible explanation for accelerating invasions, to be further tested, is that the organisms in question are sufficiently vagile as to have fat-tailed redistribution kernels. However, an alternative hypothesis is that these populations accelerate because of Allee-induced spatial thresholds (see Fig. 9).

3) The best-fitting normal redistribution kernel may grossly underestimate the speed of invasion of a spreading population in comparison with more realistic leptokurtic distributions. Since integrodifference equations with normal redistribution kernels typically yield the same speeds of invasion as simple reaction–diffusion models, it appears that simple reaction–diffusion models may also grossly underestimate speeds of invasion. This is troubling to the extent that reaction-diffusion models are the most commonly used models of spatial spread.

4) The speed of invasion of a spreading population is also dependent on the net reproductive rate for that population. Eqs. 9a, b provide us with a recipe for computing the speed of invasion as a function of the net reproductive rate. Surprisingly, redistribution kernels that are more effective in spreading a population at low net reproductive rate may be less effective at high net reproductive rates. This is most clearly seen in Fig. 4 where the speeds of invasion of probability density functions 2 and 3 (see Fig. 1) exceed that of density function 7 at low net reproductive rates but lag behind density function 7 at higher net reproductive rates.

Density functions 2 and 3 have relatively high variance. Individual propagules move far, on average, but they also have a maximum dispersal distance. Ultimately (at large R_0), the population wave speed is constrained by this maximum dispersal distance. For density function 7, individual propagules move shorter distances, on average. However, there is no maximum dispersal distance, and as R_0 increases, more and more individuals move the long distances permitted by an exponentially decaying tail: the speed of the travelling wave continues to increase with R_0.

A number of investigators have studied dispersal in which propagules are launched like projectiles. For these ballistic dispersers, propagules tend to pile up close to the maximum dispersal distance (Buller 1909, Beer and Swaine 1977, Neubert et al. 1995). In the absence of secondary dispersal, we would thus expect that, as the net reproductive rate increases, spread rates would increase rapidly and then asymptote out rapidly to the maximum dispersal distance per generation.

A great many ecologists have gone to great lengths to collect detailed dispersal data. The previous four conclusions suggest just how important these detailed data are in determining major differences in rates of spread of invading organisms. Finally, integrodifference equations appear to provide an extremely useful framework for the analysis of these data.

Acknowledgments

M. Kot wishes to acknowledge Julian Cook for thought-provoking conversations. We also wish to thank the reviewers and the editor for their detailed comments. This work was supported in part by grants from the National Science Foundation (DMS-9222371 to M. Kot, and DMS-9457816 to M. A. Lewis), from the Alfred P. Sloan Foundation (MAL), and from the Natural Sciences and Engineering Research Council of Canada (A-8965 to P. van den Dreissche). P. van den Dreissche also wishes to acknowledge the University of Victoria Committee on Faculty Research and Travel.

Literature Cited

Andersen, M. 1991. Properties of some density-dependent integrodifference equation population models. Mathematical Biosciences **104**:135–157.

Aronson, D. G., and H. F. Weinberger. 1975. Nonlinear diffusion in population genetics, combustion, and nerve propagation. Pages 5–49 *in* J. Goldstein, editor. Partial differential equations and related topics. Lecture Notes in Mathematics **446**.

Atkinson, C., and G. E. H. Reuter. 1976. Deterministic epidemic waves. Mathematical Proceedings of the Cambridge Philosophical Society **80**:315–330.

Aylor, D. E. 1986. A framework for examining inter-regional aerial transport of fungal spores. Agricultural and Forest Meteorology **38**:263–288.

Bateman, A. J. 1950. Is gene dispersion normal? Heredity **4**:353–363.

Beer, T., and M. D. Swaine. 1977. On the theory of explosively dispersed seeds. New Phytologist **78**:681–694.

Beverton, R. J. H., and S. J. Holt. 1957. On the dynamics of exploited fish populations. Fisheries Investigations Series 2(19). Ministry of Agriculture, Fisheries, and Food, London, UK.

Bowden, J., P. H. Gregory, and C. G. Johnson. 1971. Pos-

sible wind transport of coffee leaf rust across the Atlantic Ocean. Nature **229:**500–501.
Britton, N.F. 1986. Reaction-diffusion equations and their applications to biology. Academic Press, London, UK.
Brown, K., and J. Carr. 1977. Deterministic epidemic waves of critical velocity. Mathematical Proceedings of the Cambridge Philosophical Society **81:**431–433.
Buller, A. H. R. 1909. Researches on fungi. Volume I. Longmans, Green & Company, London, UK.
Bush, A. W. 1992. Perturbation methods for engineers and scientists. CRC Press, Boca Raton, Florida, USA.
Carey, P. D., and A. R. Watkinson. 1993. The dispersal and fates of seeds of the winter annual grass *Vulpia ciliata.* Journal of Ecology **81:**759–767.
Chandrasekhar, S. 1943. Stochastic problems in physics and astronomy. Reviews of Modern Physics **15**:1–91.
Clark, C. W. 1990. Mathematical bioeconomics. Wiley-Interscience, New York, New York, USA.
Dobzhansky, T., and S. Wright. 1943. Genetics of natural populations, X. Dispersion rates in *Drosophila pseudoobscura.* Genetics **28:**304–340.
Elton, C. S. 1958. The ecology of invasions by plants and animals. Methuen, London, UK.
Fisher, R. A. 1937. The wave of advance of advantageous genes. Annals of Eugenics **7:**353–369.
Fitt, B. D. L., P. H. Gregory, A. D. Todd, H. A. McCartney, and O. C. MacDonald. 1987. Spore dispersal and plant disease gradients; a comparison between two empirical models. Journal of Phytopathology **118:**227–242.
Fitt, B. D. L., and H. A. McCartney. 1986. Spore dispersal in relation to epidemic models. Pages 311–345 *in* K. J. Leonard and W. E. Fry, editors. Plant disease epidemiology. Volume 1. Macmillan, New York, New York, USA.
Gregory, P. H. 1968. Interpreting plant disease dispersal gradients. Annual Review of Phytopathology **6:**189–212.
Grove, G. G., L. V. Madden, and M. A. Ellis. 1985. Splash dispersal of *Phytophthora cactorum* from infected strawberry fruit. Phytopathology **75:**611–615.
Hardin, D. P., P. Takac, and G. F. Webb. 1990. Dispersion population models discrete in time and continuous in space. Journal of Mathematical Biology **28:**1–20.
Hassell, M. P. 1975. Density dependence in single-species populations. Journal of Animal Ecology **44:**283–295.
Hastings, A., and K. Higgins. 1994. Persistence of transients in spatially structured ecological models. Science **263:** 1133–1136.
Hengeveld, R. 1989. Dynamics of biological invasions. Chapman and Hall, London, UK.
———. 1994. Small-step invasion research. Trends in Ecology and Evolution **9:**339–342.
Howe, H. F., and L. C. Westley. 1986. Ecology of pollination and seed dispersal. Pages 185–216 *in* M. J. Crawley, editor. Plant ecology. Blackwell Scientific, Oxford, UK.
Hughes, B. D. 1995. Random walks and random environments. Volume 1. Oxford University Press, Oxford, UK.
Kable, P. F., P. M. Fried, and D. R. MacKenzie. 1980. The spread of powdery mildew of peach. Phytopathology **70:** 601–604.
Kendall, D. G. 1965. Mathematical models of the spread of infection. Pages 213–225 *in* Mathematics and computer science in biology and medicine. Medical Research Council, Oxford, UK.
Kiyosawa, S., and M. Shiyomi. 1972. A theoretical evaluation of the effect of mixing resistant variety with susceptible variety for controlling plant diseases. Annals of the Phytopathological Society of Japan **38:**41–51.
Kot, M. 1989. Diffusion-driven period-doubling bifurcations. BioSystems **22:**279–287.
———. 1992. Discrete-time travelling waves: ecological examples. Journal of Mathematical Biology **30:**413–436.
Kot, M., and W. M. Schaffer. 1986. Discrete-time growth-dispersal models. Mathematical Biosciences **80:**109–136.
Lambert, D. H., R. L. Villareal, and D. R. MacKenzie. 1980. A general model for gradient analysis. Phytopathologische Zeitschrift **98:**150–154.
Lewis, M. A., and P. Kareiva. 1993. Allee dynamics and the spread of invading organisms. Theoretical Population Biology **43:**141–158.
Lewis, M. A., and P. van den Driessche. 1993. Waves of extinction from sterile insect release. Mathematical Biosciences **116:**221–247.
Lui, R. 1982*a*. A nonlinear integral operator arising from a model in population genetics. I. Monotone initial data. SIAM Journal of Mathematical Analysis **13:**913–937.
———. 1982*b*. A nonlinear integral operator arising from a model in population genetics. II. Initial data with compact support. SIAM Journal of Mathematical Analysis **13:** 938–953.
———. 1983. Existence and stability of travelling wave solutions of a nonlinear integral operator. Journal of Mathematical Biology **16:**199–220.
Makino, S., S. Yamane, T. Sunose, and S. Aoki. 1987. Dispersion distance of queens from natal sites in the two haplometrotic paper wasps *Polistes riparius* and *P. snelleni* (Hymenoptera: Vespidae). Researches on Population Ecology **29:**111–117.
Markoff, A. A. 1912. Wahrscheinlichkeitsrechnung. Teubner, Leipzig, Germany.
McCartney, H. A., and A. Bainbridge. 1984. Deposition gradients near to a plant source in a barley crop. Phytopathologische Zeitschrift **109:**219–236.
Minogue, K. P. 1989. Diffusion and spatial probability models for disease spread. Pages 127–143 *in* M. J. Jeger, editor. Spatial components of plant disease epidemics. Prentice Hall, Englewood Cliffs, New Jersey, USA.
Mollison, D. 1972*a*. Possible velocities for a simple epidemic. Advances in Applied Probability **4:**233–258.
———. 1972*b*. The rate of spatial propagation of simple epidemics. Proceedings of the Sixth Berkeley Symposium on Mathematical Statistics and Probability **3:**579–614.
———. 1977. Spatial contact models for ecological and epidemic spread. Journal of the Royal Statistical Society **39B:**283–326.
———. 1991. Dependence of epidemic and population velocities on basic parameters. Mathematical Biosciences **107:**255–287.
Mundt, C. C. 1989. Use of the modified Gregory model to describe primary disease gradients of wheat leaf rust produced from area sources of inoculum. Phytopathology **79:** 241–246.
Mundt, C. C., and K. J. Leonard. 1985. A modification of Gregory's model for describing plant disease gradients. Phytopathology **75:**930–935.
Murray, J. D. 1977. Lectures on nonlinear-differential-equation models in biology. Oxford University Press, Oxford, UK.
———. 1989. Mathematical biology. Springer-Verlag, Berlin, Germany.
Nagarajan, S., and D. V. Singh. 1990. Long-distance dispersion of rust pathogens. Annual Review of Phytopathology **28:**139–153.
Neubert, M., M. Kot, and M. Lewis. 1995. Dispersal and

pattern formation in a discrete-time predator-prey model. Theoretical Population Biology **48:**7–43.
Okubo, A. 1980. Diffusion and ecological problems: mathematical models. Springer-Verlag, Berlin, Germany.
Okubo, A., and S. A. Levin. 1989. A theoretical framework for data analysis of wind dispersal of seeds and pollen. Ecology **70:**329–338.
Papoulis, A. 1962. The Fourier transform and its applications. McGraw-Hill, New York, New York, USA.
Pearson, K. 1905. Nature **72:**294.
Pedgley, D. E. 1986. Long distance transport of spores. Pages 346–365 *in* K. J. Leonard and W. E. Fry, editors. Plant disease epidemiology. Volume 1. Macmillan, New York, New York, USA.
Pielou, E. C. 1977. Mathematical ecology. Wiley-Interscience, New York, New York, USA.
Pomerantz, M. J., W. R. Thomas, and M. E. Gilpin. 1980. Asymmetries in population growth regulated by intraspecific competition: empirical studies and model tests. Oecologia **47**:311–322.
Prout, T. 1978. The joint effects of the release of sterile males and immigration of fertilized females on a density regulated population. Theoretical Population Biology **13:** 40–71.
Prout, T., and F. McChesney. 1985. Competition among immatures affects their fertility: population dynamics. American Naturalist **126:**521–558.
Purdy, L. H., S. V. Krupa, and J. L. Dean. 1985. Introduction of sugar cane rust into the Americas and its spread to Florida. Plant Disease **69:**689–693.
Rainey, R. C. 1973. Airborne pests and the atmospheric environment. Weather **28:**224–239.
Ricker, W. E. 1954. Stock and recruitment. Journal of the Fisheries Research Board of Canada **11:**559–623.
Rodriguez, D. J. 1988. Models of growth with density regulation in more than one life stage. Theoretical Population Biology **34:**93–117.
Roelfs, A. P. 1985. Epidemiology in North America. Pages 403–434 *in* R. Bushnell and A. P. Roelfs, editors. The cereal rusts. Volume 2. Academic Press, New York, New York, USA.
Roughgarden, J. 1986. Predicting invasions and rates of spread. Pages 179–188 *in* H. A. Mooney and J. A. Drake, editors. Ecology of biological invasions of North America and Hawaii. Springer-Verlag, New York, New York, USA.
Schieber, E. 1972. Economic impact of coffee rust in Latin America. Annual Review of Phytopathology **10:**491–510.
———. 1975. Present status of coffee rust in Latin America. Annual Review of Phytopathology **13:**375–382.
Shaw, M. 1994. Modeling stochastic processes in plant pathology. Annual Review of Phytopathology **32:**523–544.
Shigesada, N., K. Kawasaki, and Y. Takeda. 1995. Modelling stratified diffusion in biological invasions. American Naturalist **146:**229–251.
Silverman, B. W. 1986. Density estimation for statistics and data analysis. Chapman and Hall, New York, New York, USA.
Skellam, J. G. 1951. Random dispersal in theoretical populations. Biometrika **38:**196–218.
Slatkin, M. 1973. Gene flow and selection in a cline. Genetics **75:**733–756.
Southwood, T. R. E. 1978. Ecological methods: with particular reference to the study of insect populations. Chapman and Hall, London, UK.
Tarter, M. E., and M. D. Lock. 1993. Model-free curve estimation. Chapman and Hall, New York, New York, USA.
Taylor, R. A. J. 1978. The relationship between density and distance of dispersing insects. Ecological Entomology **3:** 63–70.
Thomas, W. R., M. J. Pomerantz, and M. E. Gilpin. 1980. Chaos, asymmetric growth and group selection for dynamic stability. Ecology **61:**1312–1320.
van den Bosch, F., J. A. J. Metz, and O. Diekmann. 1990. The velocity of spatial population expansion. Journal of Mathematical Biology **28:**529–565.
Wallace, B. 1966. On the dispersal of *Drosophila.* American Naturalist **100:**551–563.
Waller, J. M. 1979. The recent spread of coffee rust (*Hemileia vastatrix*) and attempts to control it. Pages 275–293 *in* D. L. Ebbels and J. E. King, editors. Plant health. Blackwell Scientific, Oxford, UK.
Weinberger, H. F. 1978. Asymptotic behavior of a model of population genetics. Pages 47–96 *in* J. Chadam, editor. Nonlinear partial differential equations and applications. Lecture Notes in Mathematics **648.**
———. 1982. Long-time behavior of a class of biological models. SIAM Journal of Mathematical Analysis **13:**353–396.
Weiss, G. H. 1994. A primer of random walkology. Pages 119–161 *in* A. Bunde and S. Havlin, editors. Fractals in science. Springer-Verlag, Berlin, Germany.
Williamson, M. 1989. Mathematical models of invasion. Pages 329–350 *in* J. A. Drake, H. A. Mooney, F. di Castri, R. H. Groves, F. J. Kruger, M. Rejmanek, and M. Williams, editors. Biological invasions: a global perspective. Wiley, Chichester, UK.
Willson, M. F. 1992. The ecology of seed dispersal. Pages 61–85 *in* M. Fenner, editor. Seeds: the ecology of regeneration in plant communities. CAB International, Wallingford, Oxon, UK.
———. 1993. Dispersal mode, seed shadows, and colonization patterns. Vegetatio **107/108:**261–280.
Wolfenbarger, D. O. 1946. Dispersion of small organisms, distance dispersion rates of bacteria, spores, seeds, pollen and insects: incidence rates of disease and injuries. American Midland Naturalist **35:**1–152.
———. 1959. Dispersion of small organisms, incidence of viruses and pollen; dispersion of fungus, spores and insects. Lloydia **22:**1–106.
———. 1975. Factors affecting dispersal distances of small organisms. Exposition Press, Hicksville, New York, USA.

APPENDIX A

1) We begin with a heuristic derivation of Eqs. 9a, b that is similar in spirit to the derivation of the wave speed for Fisher's equation (Britton 1986, Murray 1977, 1989).

Simple travelling waves that are solutions of Eq. 6 and that move to the right with velocity $c > 0$ satisfy

$$N_{t+1}(x) = N_t(x - c). \tag{A.1}$$

Near the front of any such wave we have, by Eq. 7 that

$$N_t(x - c) = R_0 \int_{-\infty}^{+\infty} k(x - y)N_t(y)\, dy, \tag{A.2}$$

where $R_0 = f'(0)$. Since Eq. A.2 is a linear equation, we look for the edge of the travelling wave to be exponential,

$$N_t(x) \propto e^{-sx} \tag{A.3}$$

with $s > 0$ so that

$$e^{-sx}e^{sc} = R_0 \int_{-\infty}^{+\infty} k(x - y)e^{-sy}\, dy. \tag{A.4}$$

The simple change of variable

$$u \equiv x - y \tag{A.5}$$

then yields the characteristic equation

$$e^{sc} = R_0 \int_{-\infty}^{+\infty} k(u)e^{su}\, du = R_0\, M(s). \tag{A.6}$$

$M(s)$ is the moment-generating function of the kernel $k(x)$ (see Eq. 8).

We are interested in monotonic (rather than oscillatory) wave fronts and real (rather than complex) roots s. Real roots emerge as a double root at the second-order contact that is given by differentiating (Eq. A.6) with respect to s:

$$ce^{sc} = R_0\, M'(s). \tag{A.7}$$

Combining Eqs. A.6 and A.7, we obtain the parametric representation

$$c = \frac{M'(s)}{M(s)} \tag{A.8a}$$

$$R_0 = \frac{e^{sM'(s)/M(s)}}{M(s)} \tag{A.8b}$$

for positive s. This curve will typically yield a minimum travelling wave speed c for each choice of net reproductive rate R_0 ($R_0 > 1$).

Initial conditions with "fat tails" may evolve into travelling waves with speeds in excess of this minimum travelling wave speed c. However, if the initial condition has compact support (is equal to zero outside some closed bounded region), the actual speed of propagation will not, in fact, be greater than c (Weinberger 1978, 1982). In particular, Eq. 4 ensures us that linearization (Eq. 7) will provide us with an upper bound for the rate of spread of a population governed by Eq. 6. Indeed, for any positive number s for which $M(s)$ is finite, define

$$c(s) = \frac{1}{s}\ln[R_0M(s)] \tag{A.9}$$

(cf. Eq. A.6). Then, if

$$N_0(x) \leq Ae^{-sx} \tag{A.10}$$

for some positive constant A, the recursion (Eq. 7) guarantees us that

$$N_1(x) \leq R_0\, M(s)Ae^{-sx}, \tag{A.11}$$

which we may rewrite as

$$N_1(x) \leq Ae^{-s[x-c(s)]}. \tag{A.12}$$

Then, by induction,

$$N_t(x) \leq Ae^{-s[x-c(s)t]}. \tag{A.13}$$

Thus, the speed of propagation is bounded above by $c(s)$. Initial conditions with compact support permit us to work with arbitrary $s > 0$. Minimizing $c(s)$ with respect to s then gives Eqs. A.8a, b.

For integrodifference equations with overcompensation or scramble competition, simple travelling waves may give way to travelling cycles or even travelling chaotic solutions (Kot 1992). However, Eqs. A.8a, b still provide an upper bound on the speed of propagation.

2) The moment-generating function $M(s)$ diverges if the redistribution kernel $k(x)$ fails to have exponentially bounded tails, and in this case, we no longer expect simple travelling waves or other constant speed solutions. However, Eq. 7 is still a valid approximation to Eq. 6 at low densities. It is natural, therefore, to try to solve Eq. 7, with an initial point source of strength N_0,

$$N_{t+1}(x) = R_0 \int_{-\infty}^{+\infty} k(x - y)N_t(y)\, dy, \tag{A.14a}$$

$$N_0(x) = N_0\delta(x), \tag{A.14b}$$

directly.

We introduce the Fourier transform,

$$\hat{N}_t(\omega) = \int_{-\infty}^{+\infty} N_t(x)e^{i\omega x}\, dx, \tag{A.15}$$

and its inverse

$$N_t(x) = \frac{1}{2\pi}\int_{-\infty}^{+\infty} \hat{N}_t(\omega)e^{-i\omega x}\, d\omega, \tag{A.16}$$

and use the fact that convolution integrals simplify under Fourier transformation. Indeed, upon Fourier transformation, Eq. A.14a reduces to

$$\hat{N}_{t+1}(\omega) = R_0\, \hat{k}(\omega)\, \hat{N}_t(\omega). \tag{A.17}$$

For our particular choice of initial condition,

$$\hat{N}_t(\omega) = N_0\, R_0^t\, \hat{k}^t(\omega), \tag{A.18}$$

for $t \geq 1$.

It is often difficult to invert Eq. A.18 directly. Instead, we analyze the Fourier transform $\hat{k}(\omega)$ and expand the exponential in this characteristic function in a Taylor series. When all of the moments of $k(x)$ are finite, we have the formal expansion

$$\hat{k}(\omega) = \int_{-\infty}^{+\infty} e^{i\omega x}k(x)\, dx = \int_{-\infty}^{+\infty} \left(\sum_{n=0}^{\infty} \frac{i^n\omega^n x^n}{n!}\right)k(x)\, dx$$

$$= \sum_{n=0}^{\infty} \frac{(i\omega)^n}{n!}\int_{-\infty}^{+\infty} x^n k(x)\, dx = \sum_{n=0}^{\infty} \mu_n' \frac{(i\omega)^n}{n!} \tag{A.19}$$

(e.g., Weiss 1994). Eq. A.18 may now be rewritten formally as

$$\hat{N}_t(\omega) = N_0\, R_0^t\, \hat{k}(\omega)\left[\sum_{n=0}^{\infty} \mu_n' \frac{(i\omega)^n}{n!}\right]^{t-1}. \tag{A.20}$$

For most kernels that have finite moments of all orders, Eq. A.19 is rigorously correct. However, we refer to Eqs. A.19 and A.20 as *formal* expansions because, for certain kernels, Eq. A.19 diverges for all nonzero values of ω. Fortunately, Eq. A.19 can then be interpreted as an asymptotic equality in the limit as ω goes to zero (Hughes 1995). (See Bush [1992] for a useful introduction to the theory of divergent asymptotic series.)

Further simplification of Eq. A.20 follows from a multinomial expansion of the bracketed term (t being an integer). However, for the general case, the resulting notation can be onerous. We begin, therefore, by showing that Eq. 18 is correct for the cases $t = 1, 2, 3$, provided that the tails of the kernel are sufficiently flat (Eq. A.27).

For $t = 1$, Eq. A.20 reduces to

$$\hat{N}_1(\omega) = N_0\, R_0\, \hat{k}(\omega), \tag{A.21}$$

and it follows trivially that

$$N_1(x) = N_0\, R_0\, k(x). \tag{A.22}$$

For $t = 2$, Eq. A.20 reduces to

$$\hat{N}_2(\omega) = N_0 R_0^2 \hat{k}(\omega)\left[\sum_{n=0}^{\infty} \mu_n' \frac{(i\omega)^n}{n!}\right], \tag{A.23}$$

or

$$\hat{N}_2(\omega) = N_0 R_0^2 \left[\sum_{n=0}^{\infty} \mu_n' \frac{(i\omega)^n}{n!} \hat{k}(\omega)\right]. \tag{A.24}$$

However, $(i\omega)^n\hat{k}(\omega)$ is just the Fourier transform of $(-1)^n d^n k/dx^n$. Hence, if we take the inverse transform of Eq. A.24 termwise, we obtain

$$N_2(x) = N_0 R_0^2 \left[\sum_{n=0}^{\infty} (-1)^n \frac{\mu_n'}{n!} \frac{d^n k}{dx^n}\right]. \tag{A.25}$$

Since $\mu_0' = 1$ for a probability density function, this may be rewritten as

$$N_2(x) = N_0 R_0^2 k(x)\left[1 + \sum_{n=1}^{\infty} (-1)^n \frac{\mu_n'}{n!} \frac{1}{k} \frac{d^n k}{dx^n}\right]. \tag{A.26}$$

In general, Expansion A.26 is of little use (Papoulis 1962); the convergence, if it occurs, is usually too slow to provide useful estimates. However, for large x, $k(x)$ decays slower than the slowest-decaying exponential (since it has no moment generating function) and faster than a negative power function (since it does have moments). A great many kernels in this class (e.g., Eq. 20) satisfy

$$\lim_{|x|\to\infty}\left[\frac{1}{k(x)} \frac{d^n k(x)}{dx^n}\right] = 0 \tag{A.27}$$

for $n \geq 1$, so that

$$N_2(x) \sim N_0 R_0^2 k(x), \qquad |x| \gg 1. \tag{A.28}$$

For $t = 3$, Eq. A.20 reduces to

$$\hat{N}_3(\omega) = N_0 R_0^3 \hat{k}(\omega)\left[\sum_{n=0}^{\infty} \mu_n' \frac{(i\omega)^n}{n!}\right]^2. \tag{A.29}$$

By employing Cauchy's rule for the product of two infinite series, we obtain

$$\hat{N}_3(\omega) = N_0 R_0^3 \sum_{n=0}^{\infty}\left[\sum_{m=0}^{n} \binom{n}{m} \mu_m' \mu_{n-m}'\right] \frac{(i\omega)^n}{n!} \hat{k}(\omega). \tag{A.30}$$

The new coefficients are, in effect, binomial convolutions of the old coefficients. Once again, $(i\omega)^n\hat{k}(\omega)$ is just the Fourier transform of $(-1)^n d^n k/dx^n$. Taking the inverse transform of Eq. A.30 termwise, we thus obtain

$$N_3(x) = N_0 R_0^3 \sum_{n=0}^{\infty}\left[\sum_{m=0}^{n} \binom{n}{m} \mu_m' \mu_{n-m}'\right] \frac{(-1)^n}{n!} \frac{d^n k}{dx^n} \tag{A.31}$$

or

$$N_3(x) = N_0 R_0^3 k(x)\left\{1 + \sum_{n=1}^{\infty} (-1)^n \left[\sum_{m=0}^{n} \frac{\mu_m' \mu_{n-m}'}{m!(n-m)!}\right] \frac{1}{k} \frac{d^n k}{dx^n}\right\}. \tag{A.32}$$

Mercifully, Eq. A.27 still applies, so that

$$N_3(x) \sim N_0 R_0^3\, k(x), \qquad |x| \gg 1. \tag{A.33}$$

We can clearly continue in this manner. For each succeeding power of the characteristic function and of the power series (Eq. A.19), we can form a Cauchy product between Eq. A.19 and the preceding power. Admittedly, the coefficients in this product will be quite complex, with binomial convolutions being replaced by multinomial convolutions, but in each instance, if the limit (Eq. A.27) is satisfied, we have

$$N_t(x) \sim N_0 R_0^t k(x), \qquad |x| \gg 1,\ t \geq 1. \tag{A.34}$$

Condition A.27, that the tails of the kernel are sufficiently flat, is at the heart of this proof. Ideally, this condition should be checked for each candidate redistribution kernel. It is true for all the kernels that we have tried that have moments but no moment-generating function and that decay monotonically in the tail. However, it is easy enough to construct kernels that oscillate in the tail and that violate Eq. A.27.

(3) Separate consideration must be given to redistribution kernels that have only a finite number of moments, but asymptotic results in such cases are still based on the characteristic function. Consider, for example, a redistribution kernel that has a stable-law form such that

$$k(x) \sim \frac{\beta^\alpha}{|x|^{\alpha+1}} \tag{A.35}$$

for large $|x|$ with β a scaling parameter and $0 < \alpha \leq 2$. It can be shown (see Weiss 1994) that for large $|x|$ the dependence of $N_t(x)$ on x is the same as that of $k(x)$.

This invariance with respect to space is especially clear for the Cauchy distribution,

$$k(x) = \frac{1}{\pi} \frac{\beta}{(\beta^2 + x^2)}, \tag{A.36}$$

which has

$$\hat{k}(\omega) = e^{-\beta|\omega|} \tag{A.37}$$

as its Fourier transform (characteristic function). In this instance, Eq. A.18 reduces to

$$\hat{N}_t(\omega) = N_0 R_0^t e^{-\beta t|\omega|}. \tag{A.38}$$

Eq. A.38 can be inverted directly,

$$N_t(x) = \frac{\beta t}{\pi(\beta^2 t^2 + x^2)} N_0 R_0^t. \tag{A.39}$$

The preservation of the large $|x|$ dependence of $N_t(x)$ is now self-evident.

APPENDIX B

We turn our attention to integrodifference equations that exhibit the idealized Allee effect of Fig. 6. However, we now consider a population that initially occupies a small interval. We define the population range at time t, $2x_t$, as that length of interval within which the population level exceeds the growth threshold N_c and we choose the space coordinate so that it is centered on the middle of this range (Fig. 9). For the piecewise constant growth dynamics of Fig. 6, we may rewrite integrodifference Eq. 6 as

$$N_{t+1}(x) = K \int_{-x_t}^{+x_t} k(x - y)\, dy. \tag{B.1}$$

A change of variables and integration yields

$$N_{t+1}(x) = K\,[F(x + x_t) - F(x - x_t)] \tag{B.2}$$

where $F(x)$ is the cumulative distribution function (CDF) defined in Eq. 26. This method of calculating the solution is shown graphically in Fig. 9. Provided that $N_{t+1}(x)$ exceeds the threshold for growth (N_c), the new population range $2x_{t+1}$ is given by Eq. B.2 as

$$F(x_{t+1} + x_t) - F(x_{t+1} - x_t) = \frac{N_c}{K}. \quad \text{(B.3)}$$

The critical spatial extent that neither increases nor decreases with time is given by

$$F(2x_c) = F(0) + \frac{N_c}{K}. \quad \text{(B.4)}$$

For the Laplace redistribution kernel,

$$k(x - y) = \frac{1}{2}\alpha e^{-\alpha|x-y|}, \quad \text{(B.5)}$$

Eq. B.2 yields

$$N_{t+1}(x) = \begin{cases} K \sinh(\alpha x_t) \exp(\alpha x), & x < -x_t \\ K[1 - \exp(-\alpha x_t)\cosh(\alpha x)], & -x_t < x < x_t \\ K \sinh(\alpha x_t) \exp(-\alpha x), & x > x_t \end{cases}. \quad \text{(B.6)}$$

If the population is invading ($x_{t+1} > x_t$),

$$\sinh(\alpha x_t) \exp(-\alpha x_{t+1}) = \frac{N_c}{K}, \quad \text{(B.7)}$$

and

$$x_{t+1} = \frac{1}{\alpha}\ln\left[\frac{K \sinh(\alpha x_t)}{N_c}\right] \quad \text{(B.8)}$$

maps the spatial extent from generation to generation. This mapping can be iterated graphically (see Fig. 10). Alternatively, if the polulation is retreating ($x_{t+1} < x_t$), we have that

$$1 - \exp(-\alpha x_t)\cosh(\alpha x_{t+1}) = \frac{N_c}{K}. \quad \text{(B.9)}$$

The decrease in spatial extent is then described by the mapping

$$x_{t+1} = \frac{1}{\alpha}\cosh^{-1}\left[\left(1 - \frac{N_c}{K}\right)\exp(\alpha x_t)\right]. \quad \text{(B.10)}$$